

On runaway breakdown and upward propagating discharges

R. Roussel-Dupré

Space and Atmospheric Sciences Group, Los Alamos National Laboratory, Los Alamos, New Mexico

A. V. Gurevich

P. N. Lebedev Institute of Physics, Moscow, Russia

Abstract. The origins of mysterious γ ray and radio flashes recently detected by satellite-based instruments passing over thunderstorms are examined in the context of upward propagating discharges initiated by runaway air breakdown. Preliminary calculations normalized by the recent optical measurements of so-called sprites indicate that the runaway mechanism may well be the source of these emissions. If this is true, then upward discharges represent the first known manifestation of a fundamental, new process in plasma physics.

1. Introduction

Sightings of optical flashes over the tops of thunderstorms have been reported sporadically for nearly a century (see Lyons and Williams [1993] for an excellent historical review) [Everett, 1903; Boys, 1926; Malan, 1937; Wilson, 1956; Gales, 1982; Vaughan and Vonnegut, 1989; Fisher, 1990]. Only recently, however, has the scientific community acquired optical measurements of sufficient quality and quantity to quantify the morphology, frequency, and brightness of the events [e.g., Franz *et al.*, 1990; Boeck *et al.*, 1990; Winckler *et al.*, 1993; Vaughan *et al.*, 1992; Vaughan, 1993; Lyons and Williams, 1993; Lyons, 1994; Sentman and Wescott, 1993; Boeck *et al.*, 1995]. Measurements have been taken from various platforms including the space shuttle, from aircraft flying near the tops of thunderstorms, and on the ground looking at storms near the horizon. In most cases the data were obtained by using low light level video imaging equipment, and the most extensive recordings were made at night for frontal type storm complexes over the U.S. midwest. The observations have yielded new and interesting information on the characteristics of these optical emissions. As described by Sentman and Wescott, events will last from <17 ms to 300 ms, occur over a height range of 25–90 km, and possess a maximum horizontal extent of 10–50 km. The emitting volume is generally >1000 km³ and has a brightness of 10–50 kR. The frequency of occurrence over large thunderstorm complexes is approximately 1 every 2 min, corresponding to a ratio of 1:500 negative cloud-to-ground flashes or 1:34 positive cloud-to-ground flashes. The more recent 1994 Colorado sprite campaign [Lyons *et al.*, 1994; Wescott *et al.*, 1995; Sentman *et al.*, 1995; Winckler *et al.*, 1994] has yielded additional information on the duration, spectrum, energetics, and dimensions of these events and has led to a distinction between two types of flashes: “blue jets,” which have a dominant blue color and extend from cloud tops to ~35-km altitude and “red sprites,” which have a dominant red color above 60-km altitude and extend to 90 km in height. Blue jets develop slowly with a vertical velocity of ≤ 100 km/s and occupy a full-angle cone of 20° just above the top of a thun-

derstorm [Wescott *et al.*, 1995]. Red sprites have a measured duration of 1–4 ms, maximum intensities of 600 kR, and lateral dimensions of tens of kilometers [Sentman *et al.*, 1995]. High time resolution photometer measurements (100-kHz sampling) have revealed temporal fine structure down to 100 μ s [Winckler *et al.*, 1994], and the maximum total energy in sprites has been measured to be several kilojoules [Sentman *et al.*, 1995]. While our understanding of optical flashes over the tops of thunderstorms has improved dramatically as a result of these newly acquired data, many questions remain regarding their nature and origin.

In 1926, C. T. R. Wilson pointed out that thunderstorm electric fields should exceed the threshold for air breakdown at altitudes above 80 km and should therefore trigger an upward propagating discharge. In 1956 he further noted that these discharges should be a regular occurrence but that the majority would be too diffuse and dim to be readily observed. The optical observations seem at first glance to support Wilson’s insightful predictions. However, one key discrepancy lies in the fact that the discharge appears to originate at low altitudes ranging from 20 to 50 km where the field strengths calculated in Wilson’s model lie well below the air breakdown threshold. Indeed, measurements of the electric field over a thunderstorm at 20-km altitude [Blakeslee *et al.*, 1989] indicate values well below the breakdown limit.

Even more intriguing are the recent satellite measurements of radio and γ ray flashes that appear to be associated with thunderstorms. First results from the Blackbeard experiment aboard the Alexis satellite [Holden *et al.*, 1995; Massey and Holden, 1995] yielded the measurement of transionospheric pulse pair (TIPP) events. These events, previously not documented in the literature, consist of a time-correlated pair of VHF spherics, separated in time by several tens of microseconds to more than 100 μ s, but having individual full widths at half maximum of 3–10 μ s and characterized by a frequency-time dispersion consistent with passage through the ionosphere. They are some 10^2 – 10^4 times more intense than radio frequency (RF) emissions from normal cloud-to-ground and intracloud lightning strokes. Although the origin of this phenomenon is presently not known, a best guess is that it is associated with lightning because of the proximity of the Alexis subsatellite point to thunderstorms when the TIPP events are detected. Another newly discovered phenomenon may also be

Copyright 1996 by the American Geophysical Union.

Paper number 95JA03278.
0148-0227/96/95JA-03278\$05.00

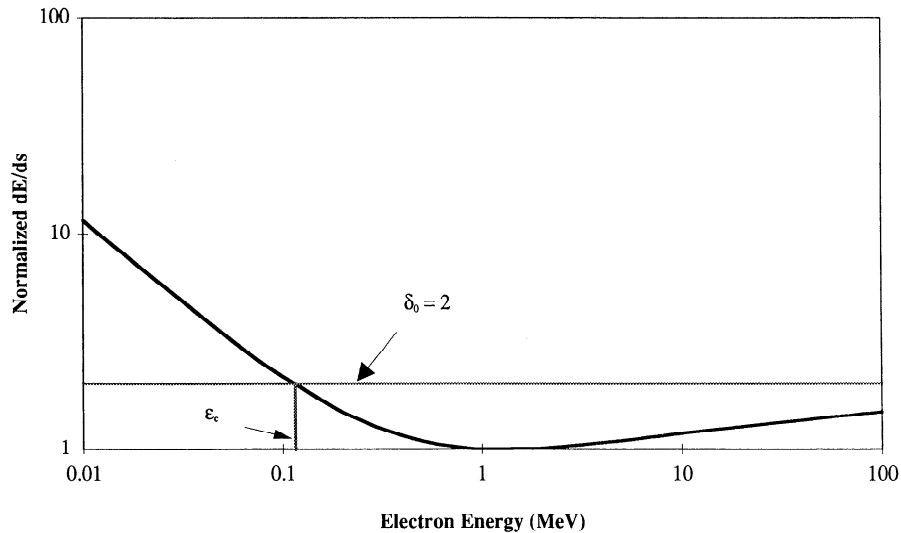


Figure 1. Rate of electron energy loss in air. The frictional drag dE/ds experienced by an electron as it propagates through air is plotted as a function of the electron energy.

related to high-altitude discharges, but again, corroborating optical observations were not available to make a definitive association. Bursts of intense, hard γ ray emission from the atmosphere were observed by the Burst and Transient Signal Experiment (BATSE) aboard the Compton Gamma Ray Observatory (CGRO) when the subsatellite point was above large thunderstorm complexes near the equator [Fishman *et al.*, 1994]. The events generally contained multiple (up to four), short (rise and fall times between 0.1 and 2 ms), intense (energy fluences between 10^8 and 10^9 ergs), and high-energy (consistent with a bremsstrahlung spectrum having 1-MeV characteristic energy) pulses. Although only 12 confirmed events were observed in 2 years, the high threshold and operational characteristics of the trigger circuit of the BATSE experiment, which was set for cosmic γ ray bursts, may have missed potentially many more of a general category of atmospheric γ ray bursts. The association of these emissions with the optical flashes stems not only from the proximity of the subsatellite point to thunderstorm activity but also from the fact that strong atmospheric absorption and scattering limit the source region to altitudes above 25 km, a finding that happens to coincide well with the altitude range of the optical measurements.

If the γ ray measurements obtained by BATSE can be directly linked to the sprites and blue jets defined by the optical observations, then we must rule out the Wilson model and any model that is based on conventional air breakdown [e.g., Taranenko *et al.*, 1993a, b; Milikh *et al.*, 1995; Rowland *et al.*, 1995; Pasko *et al.*, 1995]. An alternative solution for the initiation of upward discharges is rooted in the runaway air breakdown mechanism, and the purpose of this paper is to illustrate how this mechanism can account for both the γ ray and radio flashes and for the optical measurements of sprites. In this paper we use the measured total optical energy to normalize the magnitude of the runaway beam. From simple analytic estimates for the beam evolution in the background atmosphere and a model for the thunderstorm-generated electric field we then compute numerically the corresponding optical intensity profile and the associated γ ray and VHF electromagnetic emissions. A more detailed two-dimensional

hydrodynamic model has been developed by Taranenko and Roussel-Dupré [1996] to treat the beam and secondary electrons. However, this model does not attempt to calculate the VHF emissions. In addition, we have taken a simpler, semiempirical approach here in order to better elucidate the essential physics and to emphasize the general role that runaway breakdown can play in initiating thunderstorm discharges.

A review of the salient features of runaway breakdown is provided in section 2 together with a general quantitative analysis of the breakdown morphology and the emissions expected from a discharge of this type. The results of our calculations are then applied in section 3 to the development of a rough model for upward discharges. A summary of our findings is provided in section 4.

2. Runaway Breakdown

Basic Description

Runaway breakdown was first described in a paper by Gurevich *et al.* [1992]. A more detailed kinetic treatment that describes the temporal evolution of the electron distribution function in a uniform background electric field is presented by Roussel-Dupré *et al.* [1994]. The basic elements of this mechanism are rooted in the well-known fundamental works of Bethe [Bethe, 1930; Bethe and Ashkin, 1953] on high-energy particle interactions with matter. To illustrate how runaway breakdown proceeds, we have plotted the frictional force experienced by high-energy electrons in air as a function of electron energy in Figure 1. We see that a minimum exists at approximately 1 MeV. Clearly, if an electric force whose magnitude exceeds the minimum is applied to the medium, then electrons with energies greater than the critical value ϵ_c at which the electric force equals the frictional force (see Figure 1) will be maintained and accelerated (runaway) to higher energies. While Wilson [1925, 1956] and more recently McCarthy and Parks [1992] appreciated this fact and studied its effects in the context of thunderstorm electric fields, they overlooked the possibility that an avalanche might develop: It is also well known that

impact ionization of the air by energetic electrons will lead to the production of energetic secondary electrons. Those secondary electrons whose energies exceed the critical value ε_c become part of the runaway population and contribute to further ionization that also populates the runaway regime. The net result is an avalanche in which the electron population grows exponentially. Collimation of these relativistic electrons by the electric field leads to the formation of an electron beam, which grows exponentially as it propagates through the medium as long as the electric field exceeds the threshold defined by the minimum of the frictional force.

While these results have been substantiated by detailed calculations, experimental validation is not presently available, primarily because of the large (on a laboratory scale) dimensions (tens to hundreds of meters at sea level) required for the avalanche to develop. Nevertheless, the sheer simplicity of the mechanism and the fact that it is founded on such well-known physical principles argue strongly in favor of its existence. In addition, the large-scale lengths and electric potentials associated with thunderstorms provide ideal conditions for development of runaway breakdown, and indeed, the recent measurements of upward discharges may well be the first available evidence for its existence.

One important feature of this mechanism is that the threshold electric field needed to initiate the avalanche lies a factor of 10 below that for conventional breakdown (as observed in the laboratory). Interestingly, macroscopic field strengths exceeding the threshold for conventional breakdown have never been measured in thunderstorms, while values near and exceeding the threshold for runaway breakdown have often been measured [see Winn *et al.*, 1974, 1981; Uman, 1984; Krehbiel, 1986; Marshall and Rust, 1991]. With these facts in mind we can view the evolution of thunderstorm electric fields and the preconditioning stage of lightning discharges in a new light. As cloud electrification proceeds, the electric field in a thunderstorm slowly grows in amplitude in the weakly conducting background atmosphere until the threshold for runaway is exceeded. At this point, many discharges are initiated, and depending on the range and configuration of the field, sufficient current can be generated to limit the field strength to the threshold level. At 5 km the threshold field is approximately 100 kV/m, whereas the value at 10 km is 50 kV/m. Vertical soundings (see previous references) of the electric field in thunderstorms tend to support this picture. In cases where the field grows more rapidly than neutralizing currents can develop, the threshold for runaway is exceeded by a larger factor, which in the presence of sufficient field range results in strong discharges that deposit a substantial amount of charge hundreds of meters to kilometers from the initiating charge layer. This new charge region can itself drive a runaway discharge, and in this way the runaway mechanism can cause the development of an electrical channel that preconditions the atmosphere for a lightning discharge (return stroke in the case of cloud-to-ground lightning). More quantitative estimates of these effects can be found in a report by Roussel-Dupré *et al.* [1993]; however, much theoretical and experimental work remains in order to substantiate this basic picture.

One of the unique signatures of runaway breakdown is the strong γ ray flux produced by the beam interaction with air. Unfortunately, γ rays are also readily absorbed in air, and the detection of such emissions necessitates a distance to the discharge of less than several hundred meters to 1 km at sea level, depending on the strength of the discharge. At high altitudes

Table 1. Electron Beam Parameters

Case	$\delta_0 = 1.5$	$\delta_0 = 2.0$	$\delta_0 = 5.0$	$\delta_0 = 8.0$
Avalanche time pressure, ns/atm	53.8	14	3.5	1.5
Mean energy, MeV	1.6	0.95	1.2	0.82
Energy spread, MeV	2.0	1.45	1.9	1.4

above 25 km the atmosphere becomes transparent to these emissions, and remote detection becomes feasible. In addition, because the frictional drag on electrons decreases exponentially with height and the dipole field from thunderstorms decays slowly (as $1/r^3$), the threshold for runaway is more easily exceeded over larger distances at high altitude. As a result, runaway breakdown is more likely to be detected in high-altitude discharges. Indeed, we believe that the γ rays detected by BATSE originate from the same upward propagating discharges that are observed as sprites and blue jets.

In concluding this section we would like to emphasize that the basic form of the frictional force derived by Bethe [1930] has application to all forms of matter (solids, liquids, and gases) and that runaway breakdown may therefore have its manifestation in many different natural phenomena.

Physical Characteristics

The basic properties of the electron beam formed in runaway breakdown such as its mean energy, velocity, energy spread, and avalanche rate depend on the magnitude of the applied electric field divided by the atmospheric pressure (E/p) or equivalently in terms of the parameter $\delta_0 = E/E_t$, where E_t is the magnitude of the threshold electric field for runaway breakdown. The threshold field is given by $E_t = 218 (p/p_0)$ kV/m [Gurevich *et al.*, 1992; Roussel-Dupré *et al.*, 1994], where p is the atmospheric pressure and p_0 is the pressure at sea level. A summary of the runaway beam characteristics obtained from detailed kinetic calculations is shown in Table 1 for four values of δ_0 .

The spatial diffusion of the electron beam due to scattering was described by Gurevich *et al.* [1994]. The results indicate that the beam is constrained to move along the electric field with a lateral diameter $D \approx 30 (2/\delta_0)^2 (p_0/p) (\eta/\eta_0)^{1/2} m$, where η is equal to the total number of e -foldings of the beam population and $\eta_0 = 40$. A plot of D as a function of altitude for $\delta_0 = 2, 5$, and 8 and $\eta = \eta_0$ is shown in Figure 2. The length of the beam along the electric field is $L \approx 68 (p_0/p) (\eta/\eta_0) m$ and is also shown as a function of height for $\eta = \eta_0$ in Figure 2.

The electron beam formed as a result of runaway breakdown collides with air molecules, causing them to fluoresce in the visible part of the electromagnetic spectrum. At the same time these collisions scatter the beam electrons, causing them to slow down and to emit bremsstrahlung radiation (braking radiation). Electrical breakdown of the air also leads to the formation of low-energy, secondary electrons, which in turn accelerate in the thunderstorm field. Together the beam and secondary electron populations carry a significant current that changes rapidly in time and results in the production of radio waves. The magnitudes of these emissions depend explicitly on the field strength δ_0 , the total number of avalanche lengths η , and the air pressure p . The optical, γ ray, and radio fluxes are estimated below.

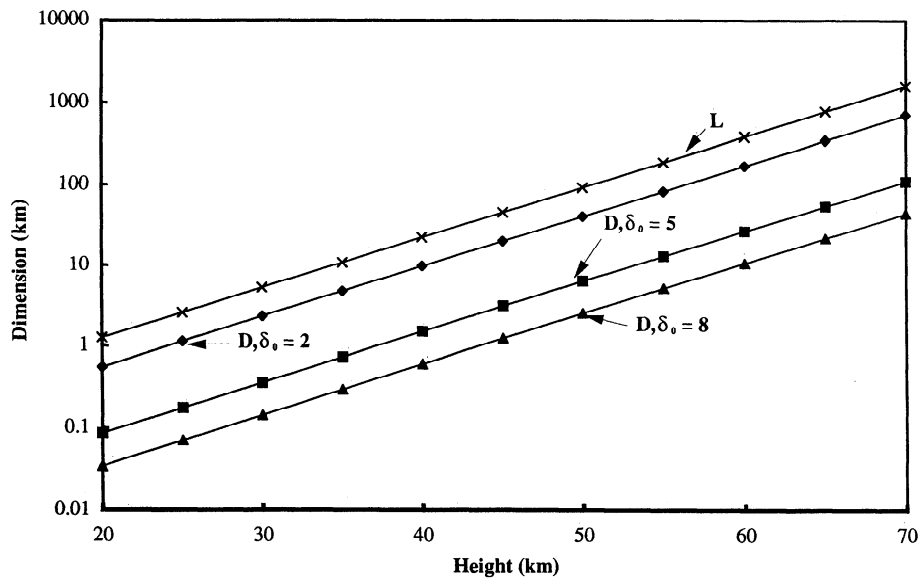


Figure 2. Diameter and length of discharge. The maximum diameter of the runaway discharge region after 40 avalanche lengths is plotted as a function of height for three values of $\delta_0 = 2, 5,$ and 8 . The length of the discharge region is independent of δ_0 to a first approximation and is also plotted as a function of height.

Optical Emissions

Given the total energy of the runaway electron beam, it is possible to calculate the optical emissions based on the air fluorescence efficiencies measured by Davidson and O'Neil [1964], Hartman [1968], and Mitchell [1970]. The efficiencies are known over the entire optical range and into the ultraviolet (250–1000 nm) and are independent of the beam energy in the energy range of interest. The fluorescence efficiency χ is defined to be the optical energy or power divided by the beam energy or power deposited in air. The energy deposited by the beam is equal to its total energy simply because the electric field is constantly doing work against friction to maintain the electrons. Davidson and O'Neil give $\chi = 0.01$ for the band from 330 nm to 900 nm at low pressures ($p < 0.1$ torr). A general expression that accounts for quenching at high pressures is $\chi = 0.01/(1 + 1.13 p)$, where p is the atmospheric pressure in torr. From the spectra provided by Davidson and O'Neil and the results of Mitchell it is also possible to derive efficiencies for various wavelength bands. A plot of the efficiencies as a function of altitude is provided in Figure 3. Note that the red emissions begin to dominate at altitudes above approximately 60 km in agreement with observations of red sprites [Sentman et al., 1995].

Thus total optical energy produced by runaway air breakdown in various bands can be written

$$W_o \approx 1.6 \times 10^{-19} \chi N \langle \varepsilon \rangle \quad \text{J} \quad (1)$$

where N is the total number of electrons in the electron beam and $\langle \varepsilon \rangle$ is the average energy of the beam electrons in eV. Equation (1) can be rewritten in such a way as to separate out the explicit pressure dependence. For the entire band from 330 to 900 nm we find

$$W_o \approx \frac{1.6 \times 10^{-21} N_0 e^{\eta \langle \varepsilon \rangle}}{1 + 1.13 p} \quad \text{J} \quad (2)$$

where N_0 is the number of high-energy electrons that initiate the breakdown. A plot of $W_o(1 + 1.13 p)$ versus η with $N_0 =$

1 is provided in Figure 4 for $\delta_0 = 2, 5,$ and 8 . Note that if we omit the ultraviolet lines, the magnitude of the emissions drops by a factor of 3–5. We also point out that W_o has only a very weak dependence on δ_0 through $\langle \varepsilon \rangle$. Thus these results can be used in conjunction with the observed emissions from upward discharges to obtain a value for $N_0 e^{\eta}$ or an effective η , such that $\eta_{\text{eff}} = \eta \ln N_0$.

The γ Ray Emissions

The flux of γ radiation expected from a single runaway discharge and measured at a distance R from the source can be written

$$F_v \approx \frac{\varepsilon_v V_s e^{-\rho \mu R}}{R^2} \quad \text{photons/cm}^2 \text{ s eV} \quad (3)$$

where ε_v is the emissivity of the discharge volume for photons of energy $h\nu$, V_s is the source volume, ρ is the air mass density, and μ is the absorption coefficient (in cm^2/g) for photons of energy $h\nu$. The emissivity

$$\varepsilon_v = 2N_m \int dp p^2 \int d\Omega f(p, \mu) \frac{d^2 \chi_R}{dv d\Omega} \beta c. \quad (4)$$

where $f(p, \mu)$ is the self-similar electron velocity distribution function obtained from detailed kinetic calculations, N_m is the air number density, and $d^2 \chi_R/dv d\Omega'$ is the Bethe-Heitler doubly differential cross section for bremsstrahlung emission by a relativistic electron. The reader is referred to Roussel-Dupré et al. [1994] for details. Because ε_v is proportional to the electron density, the product $\varepsilon_v V_s$ is proportional only to the total number of electrons, i.e., varies as e^{η} .

To calculate the average γ flux measured by an observer at a distance R from the source and located at an angle θ relative to vertical, equation (3) is first integrated over time (or height), assuming that a runaway discharge initiated by a single high-energy electron is developing vertically upward along the thunderstorm electric field. The resulting integral is then divided by

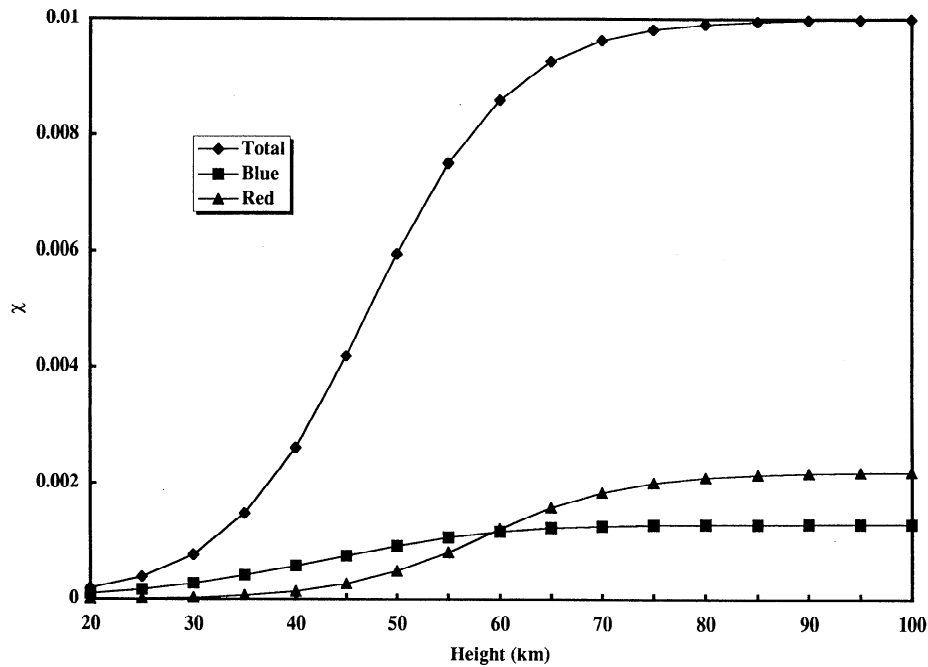


Figure 3. Fluorescence efficiencies. The fluorescence efficiencies for the optical plus ultraviolet emissions resulting from electron impact excitation of air by an energetic electron beam are plotted as a function of altitude. The efficiencies are plotted for three spectral bands: total optical plus ultraviolet (300–900 nm), blue (N_2 2P emissions from 400 to 500 nm plus N_2^+ 1N emissions from 400 to 500 nm), and red (N_2 1P emissions from 600 to 700 nm).

the total duration of the event to obtain an average flux. The flux at a distance of 500 km from the source was computed in this way for several values of δ_0 ($= 2, 5,$ and 8) and for several angles θ ($= 0^\circ, 30^\circ,$ and 60°), assuming that δ_0 remains constant while all other parameters vary with height or atmospheric pressure. The results plotted as a function of γ ray energy for $\delta_0 = 2$ and for start altitudes of 25, 26, and 27 km are presented in Figures 5a, 5b, and 5c, respectively. Note that the γ ray flux

is very sensitive to the altitude at which runaway breakdown is initiated because of the rapid increase in both the avalanche length and the photon absorption scale length with height.

Radio Emissions

The radio emissions from runaway breakdown as measured by a distant observer are estimated by adopting a simplistic representation for the primary and secondary currents pro-

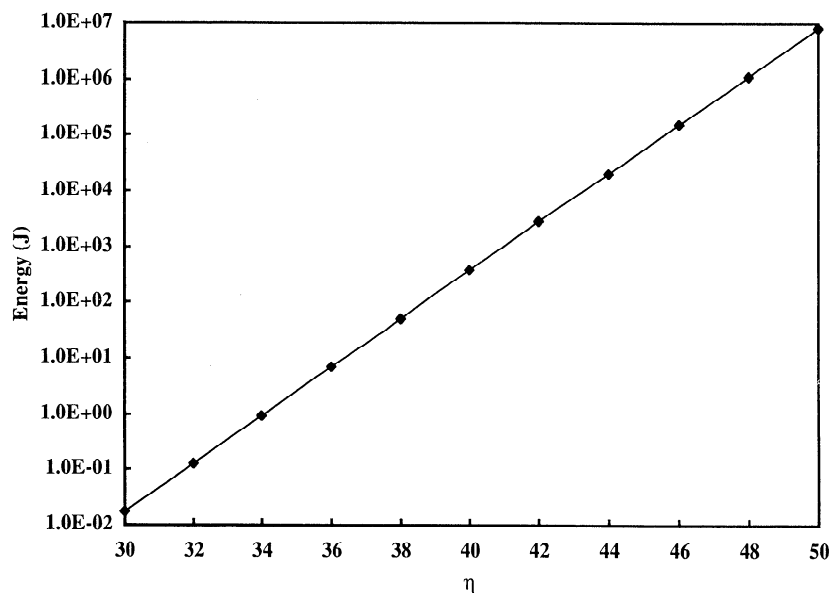


Figure 4. Optical energy. The total scaled optical energy [$W_0(1 + 1.13 p)$] emitted during the passage of an electron beam through air is plotted as a function of the number of beam avalanche lengths. Read 1.0E-07 as 1.0×10^{-7} .

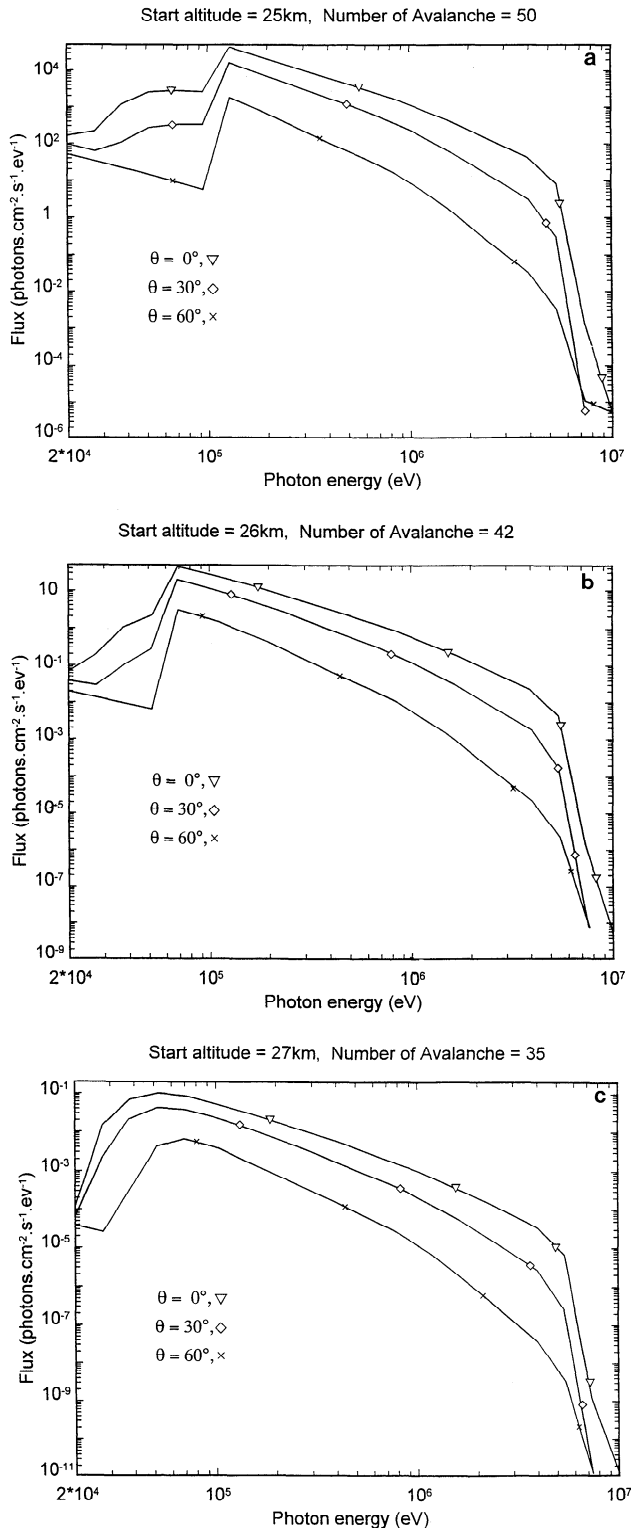


Figure 5. Bremsstrahlung flux. The flux of γ ray photons produced by runaway air breakdown and observed at 500 km from the source and angles of 0° , 30° , and 60° from vertical is plotted as a function of γ ray energy for three start altitudes: (a) 25 km, (b) 26 km, and (c) 27 km.

duced in the discharge. The relativistic electron beam is approximated as a single primary charge with a magnitude $Q_p = -N_p e$ (where N_p is the total population of primary electrons produced in the breakdown and e is the charge of a proton)

that grows at the avalanche rate v . The primary charge is assumed to move with a constant relativistic velocity v_p . The low-energy secondary electrons are represented as a single charge whose instantaneous magnitude in the frame of the beam $Q_s = (e_p/e_f) Q_p$, where e_p is the mean energy of the runaway beam electrons and e_f ($= 34$ eV in air) is the energy expended per ion pair produced. The secondary charge moves with a drift velocity v_s defined by the balance between the field acceleration and the frictional deceleration. The positive ions are represented as a single stationary charge with instantaneous magnitude $Q_i = -(Q_p + Q_s)$. With this simple representation it is possible to use the Lienard-Wiechart potentials to compute the radiation fields. The flux measured at a distance R from the source and an angle θ relative to the direction of motion of the electron beam (or relative to vertical in upward propagating discharges) is found to be

$$F_R = \frac{c}{4\pi} \left(\frac{e v}{R c} \right)^2 \frac{\beta_p^2 e^{2n} \sin^2 \vartheta}{(1 - \beta_p \cos \vartheta)^4} \left(1 + \frac{\varepsilon_p \beta_s}{\varepsilon_1 \beta_p} \frac{1 - \beta_p \cos \vartheta}{1 - \beta_s \cos \vartheta} \right)^2, \quad (5)$$

where $\beta_{p,s} = v_{p,s}/c$. Note that the flux is proportional to the avalanche rate squared and that a significant forward peaking of the radiation results for the contribution from the relativistic beam. A plot of $\sin^2 \theta / (1 - \beta_p \cos \theta)^4$ is provided in Figure 6. The peak emission for the beam occurs at approximately $\theta_p = 13^\circ$ with a full width at half maximum of about 20° . The contrast in emission between θ_p and 90° is about a factor of 1000. The contribution of the secondary electrons increases rapidly with angle and is in general important over nearly the entire angular range. A plot of the angular distribution including the effect of secondaries when $\delta_0 = 2$ ($\beta_s/\beta_p = 10^{-4}$) is also shown in Figure 6. Note that the radiation is much less sharply peaked, and the contrast between the peak emission and that at 90° is now only a factor of approximately 100.

Taking the Fourier transform of the calculated electric field and multiplying by the corresponding complex conjugate yields a function that falls off as $1/[v^2 + (1 - \beta_p \cos \theta)^2 \omega^2]$. The avalanche rate v in air has a value that ranges from 20 to 600 MHz at sea level to 0.5 to 20 MHz at 25-km altitude. Thus thunderstorm discharges initiated by the runaway mechanism will produce significant amounts of VHF radiation. We note that the relativistic nature of the source further enhances the high-frequency component of the emissions depending on the angle of the observer, as reflected in the factor $(1 - \beta_p \cos \theta)^2$. At frequencies much greater than v the flux drops off slowly as $1/\omega^2$.

Effect of the Geomagnetic Field

The magnetic field becomes important in the development of runaway breakdown when the electron gyrofrequency equals or exceeds the angular scattering rate. For $\delta_0 = 2$ this condition is met at altitudes above 40 km. As δ_0 increases, the runaway population becomes more collision dominated (the critical energy ε_c drops to values where collisions become more important), and the condition is met at higher altitudes, 50–60 km. In order for the electrons to run away in energy in the presence of a magnetic field the electric field component along the magnetic field must at the very least exceed the threshold. In latitude regions where the dip angle of the magnetic field is large the latter condition will be more easily satisfied, and runaway will generally proceed with minor modifications. However, at lower latitudes the increased path

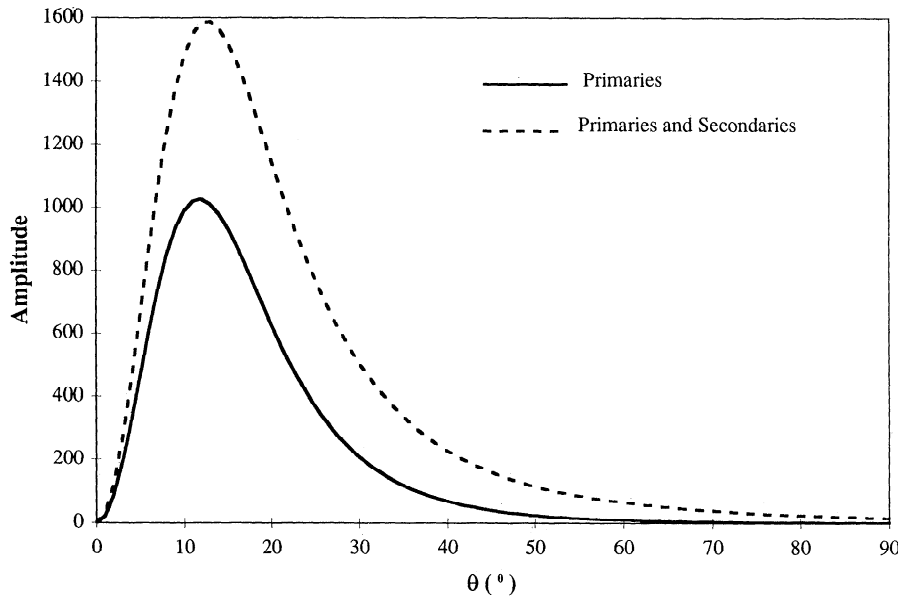


Figure 6. Angular distribution of radio emissions. The quantity $\sin^2 \theta / (1 - \beta_p \cos \theta)^4$, corresponding to the angular factor for radio emission by primaries, is plotted as a function of angle θ (solid line). The angular factor including the contribution from secondaries is also plotted as a function of angle θ (dashed line).

length due to particle gyration leads to energy loss, and runaway is quenched. Nevertheless, the fact that electrons no longer run away does not mean that the avalanche is quenched. Indeed, in a process called thermal runaway the redistribution in angle of the electrons by the magnetic field acts together with scattering and the electric field to maintain a population of high energy electrons with a net increase in the avalanche rate. Detailed kinetic calculations [Roussel-Dupré and Miller, 1994] of this process show enhancements by as much as a factor of 10 in the regime where the gyrofrequency equals the scattering rate. Thus the magnetic field will be important at low geomagnetic latitudes and high altitudes, changing both the basic nature and the development of the discharge. We note that the gyration of the energetic electrons at high altitudes will result in low-frequency (<1 MHz) radiation not considered in this paper.

3. Model of Upward Discharges

As was shown in the previous section, the basic characteristics of runaway breakdown are defined entirely in terms of two parameters, δ_0 and η . Thus, given a representation for the electric field above a thunderstorm (δ_0) and an estimate for the total number of electrons in the discharge or in an equivalent single runaway beam (i.e., $N = N_0 e^\eta$), it is possible to specify the basic properties of the discharge. The method used to determine these parameters is described below.

Our model for upward propagating discharges begins with a simple electrostatic dipole representation for the thunderstorm electric field. We allow for currents within the conducting atmosphere to establish a counter polarization field so that the net field is the sum of the thunderstorm electric field plus the polarization field $\mathbf{E} = \mathbf{E}_T + \mathbf{E}_P$. We then simulate a cloud-to-ground or intracloud flash by neutralizing a portion of the dipole charge in a time τ , which results in a corresponding decrease in the thunderstorm electric field. For an atmosphere with a finite conductivity we obtain the following expression for

the resulting electric field as a function of height h along the axis of the dipole,

$$\delta_0 = \frac{Q}{E_t} \left[\frac{1}{(h - h_+)^2} - \frac{1}{(h - h_-)^2} \right] \frac{1}{1 - 4\pi\sigma\tau} \cdot [e^{-4\pi\sigma\tau} - e^{-t/\tau}] e^{h/H}, \quad (6)$$

where Q is the magnitude of the charge, h_+ (h_-) is the altitude of the positive (negative) charge layer, σ is the conductivity of the atmosphere, H is the atmospheric scale height (taken to be 7 km), and E_t is the threshold electric field for runaway at sea level. Because the background conductivity cannot respond to the change in field strength (which occurs over tens of milliseconds), the remaining field is dominated by the polarization field in the region above the neutralized charge. If the charge that is neutralized is primarily positive (for example, the transfer of negative charge to the top of the cloud via an intracloud strike), then the net field will point downward so that electrons are accelerated upward. The magnitude of the neutralized charge will determine the altitude and extent of the region that lies above the threshold for breakdown. A sketch of this basic model is shown in Figure 7. In addition, we plot the electrical relaxation time for the background atmosphere as a function of height in Figure 8. For a nighttime atmosphere the values exceed 1 ms for altitudes below 70 km. Above 70 km the polarization fields will be shorted out on rapid timescales. In the daytime this altitude drops to 60 km. At altitudes below 55 km the relaxation time exceeds 100 ms for both day and nighttime conditions.

The magnitude and distribution of the net field form the initial condition for the discharge. As an example, suppose that a layer of positive charge located at the top of a giant thunderstorm possesses a total charge of 100 C distributed over a 1-km-diameter spherical region at 18-km altitude and that a similar negative charge distribution exists at 5-km altitude. Assuming that an intracloud stroke neutralizes this region of charge in a timescale of the order of 10 ms, the resulting

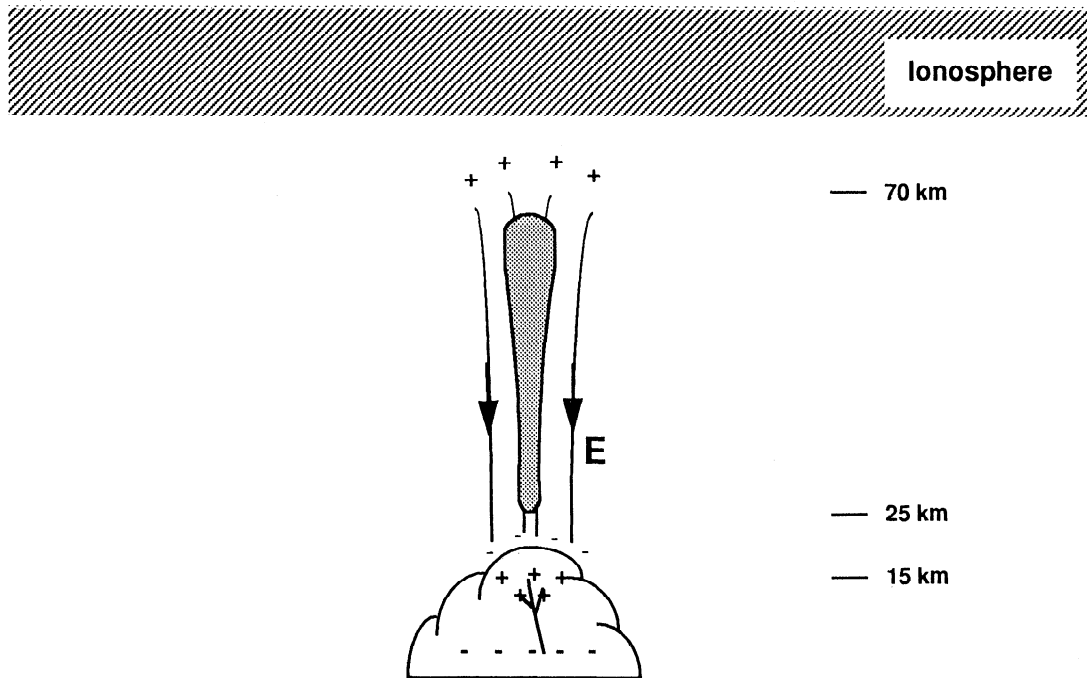


Figure 7. Model of upward propagating discharges. A cartoon depicting the electric field configuration above a thunderstorm following an intracloud strike and the ensuing development of a runaway upward discharge is shown.

polarization field normalized to the local threshold electric field (E_t) will have the magnitude shown in Figure 9 along the vertical axis of the dipole as a function of height for the nighttime conductivity profile shown in Figure 8. The latter results correspond to a snapshot of the field at the time when the field is a maximum at 25-km altitude. We find that the threshold for runaway is exceeded throughout the altitude range above the cloud up to approximately 65 km. Above 75 km the threshold for conventional breakdown would also be exceeded, as predicted by *Wilson* [1925], were it not for the high electrical relaxation rate of the atmosphere in this region.

Although one can argue about the detailed charge configuration, the thunderstorm conditions discussed above are not extreme. As discussed by *Uman* [1984, pp. 96–101 and references therein], measurements of cloud discharge moment changes of several hundred coulomb kilometers have been reported. In addition, charge neutralizations of 100 C have been found to occur quite often in intracloud discharges. Positive cloud-to-ground discharges which neutralize the positive charge in a cloud will have the same effect as the intracloud discharge in our model, namely, there will be an enhancement in the negative electric field above the cloud. These discharges have been measured to lower an average charge of 87 C [*Uman*, 1984, p. 125] in less than 200 ms. More recently, positive ground flashes with “extraordinarily” large dipole moment changes have been found to occur “systematically” in association with “sprites,” as noted by *Bocchippio et al.* [1995].

While many discharges can be initiated over the entire region where the threshold fields are exceeded, the dominant observationally will be those that are initiated at the lower altitudes, because they will develop over many avalanche

lengths. To illustrate this fact, we plot in Figure 10 the number of avalanche lengths between a start altitude H_s and 100-km altitude as a function of H_s for $\delta_0 = 2, 5,$ and 8 , assuming that the avalanche develops vertically and that δ_0 remains constant with height. Note that the number of avalanche lengths decreases rapidly with height. Given that the polarization field points downward in this case, we expect an observable upward discharge to start at low altitude ($H \sim 25$ km) and proceed upward. One consequence of this result is that the discharge spatial characteristics at higher altitudes will be defined by the diffusion of the electron beam rather than the dimensions of the source region in which the threshold field is exceeded, provided the latter region is larger than the beam dimensions. In addition and more important, the electrical relaxation times are much larger at lower altitudes, and therefore the currents required to neutralize the 100 C needed to initiate these discharges is substantially reduced.

To proceed further, we will use the magnitude of the optical observations of sprites and the results presented in Figure 4 to determine the number of avalanche lengths or the strength of the beam. Taking an observed flux $F_{\text{obs}} = 25$ kR over a 17-ms integration time and an emitting surface area of 100 km^2 [see *Sentman and Wescott*, 1993], we obtain $W_{\text{obs}} \approx 175$ J for the total optical energy. More recent measurements have yielded values corresponding to several kilojoules. In order to allow for emission processes not included in our model (see discussion below) we will normalize the beam strength to 500 J of total optical energy. Given the total number of avalanche lengths η as a function of height (or pressure, p) from Figure 10 and the energy as a function of η and p from Figure 4 (essentially two equations in two unknowns), we can determine values for p

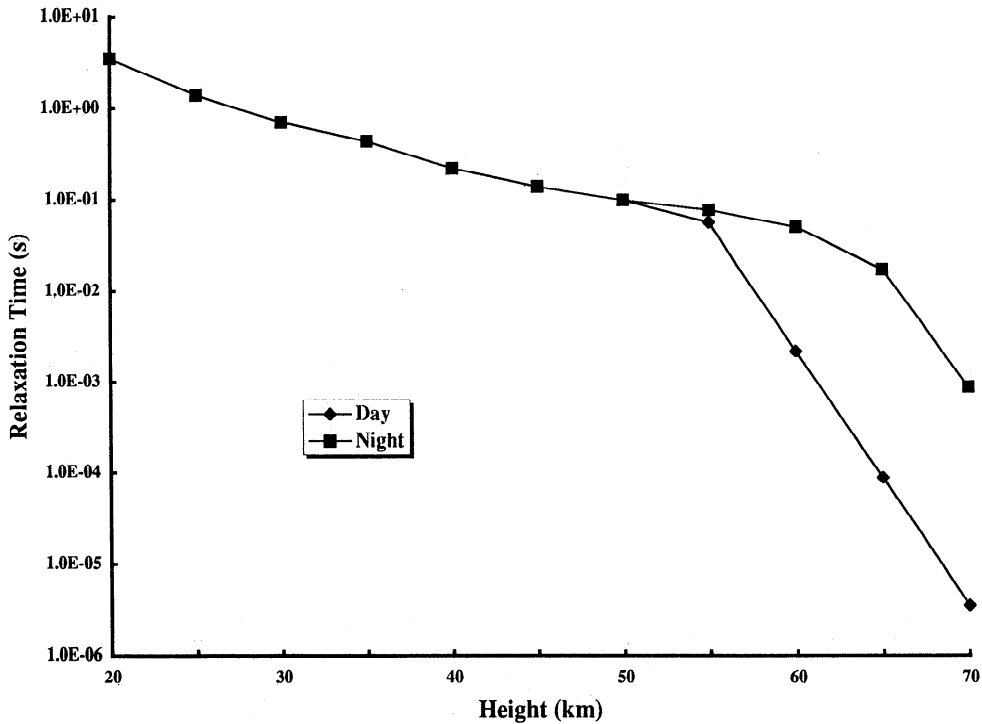


Figure 8. Electrical relaxation times. Typical electrical relaxation times for a daytime and a nighttime atmosphere are plotted as a function of altitude.

and η that are independent of δ_0 . Taking into account that the cameras used to measure these discharges have poor sensitivity in the ultraviolet, we find $\eta_{\text{eff}} = 41.5$ and $p = 19$ torr or $H_s = 26$ km.

Thus the basic picture of the discharge that emerges from these calculations can be summarized as follows. Following an intracloud or positive cloud-to-ground flash of sufficient

strength (e.g., 100 C of charge neutralized in 10 ms), an electric field that exceeds the threshold for runaway breakdown is established above the neutralized charge region up to 65-km altitude. Energetic electrons produced by cosmic ray interaction with the air accelerate and avalanche in the presence of this field. Though many individual discharges are initiated, only those that start at low altitudes will develop over sufficient

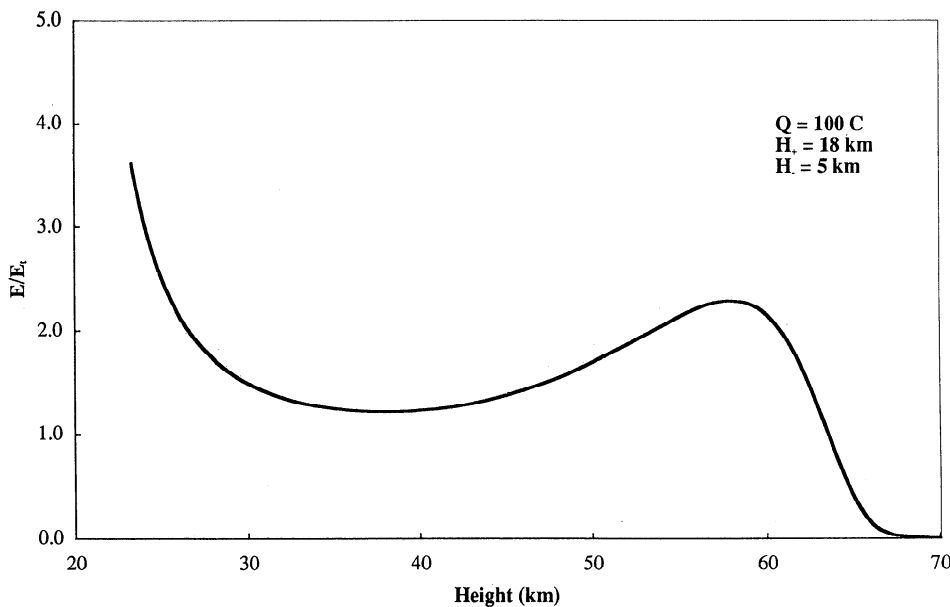


Figure 9. Thunderstorm electric field. The normalized magnitude of the electric field above a thunderstorm following an intracloud strike that neutralizes 100 C of charge in 10 ms is plotted as a function of altitude for a time when the field maximizes at 25-km altitude. The values plotted here are for the altitude range along the axis of the neutralized charge.

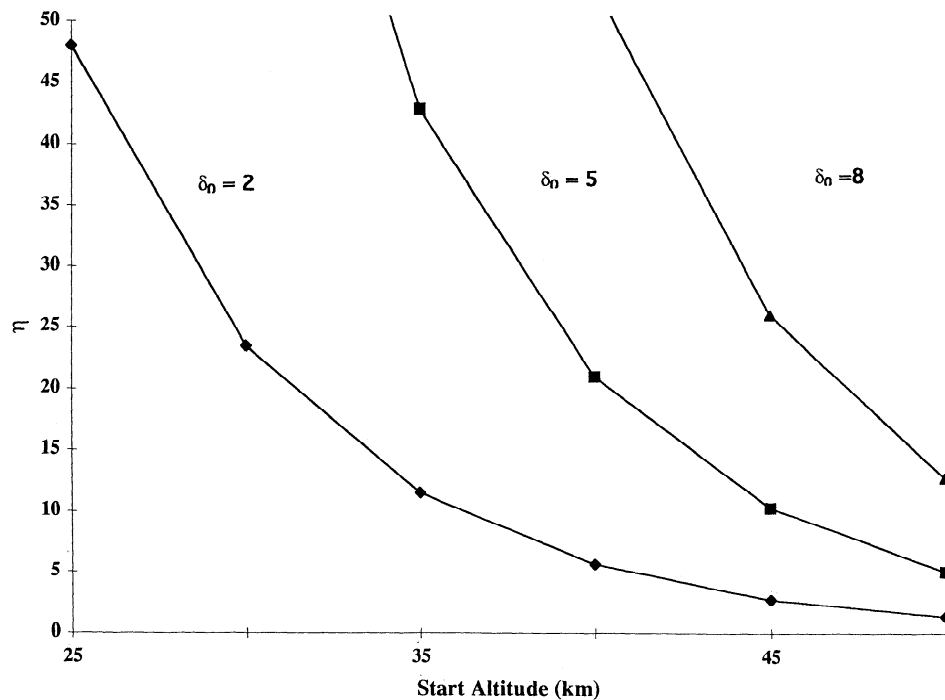


Figure 10. Number of avalanche lengths. The total number of avalanche lengths that develop between the start altitude (H_s) of a runaway discharge and 100-km altitude (or infinity) is plotted as a function of start altitude for three values of $\delta_0 = 2, 5,$ and 8 .

avalanche lengths to be observed. The optical observations can be used to determine the total energy (total number of electrons) in the overall discharge and indicate that an equivalent discharge initiated by a single energetic electron requires over 40 e -foldings in order to account for the observed emissions. This requirement then sets the altitude at which the avalanche was initiated. This basic scenario is illustrated in Figure 7.

With the value of η specified, it is now possible to obtain all of the parameters associated with the runaway breakdown region. The total energy contained in the electron beam ($=e^\eta \langle \epsilon \rangle$) is approximately 170 kJ. The diameter of the dis-

charge region as a function of height is shown in Figure 11. At 60-km altitude we obtain a diameter of 28 km, which lies within the observational range of 10–50 km. The corresponding profile of optical intensity is shown in Figure 12. Note that there are two peaks. The strong, first peak (~ 27 MR) results from the small dimensions (< 1 km in diameter) and fast timescales (~ 1 - μ s risetime) associated with the low-altitude portion of the discharge. The observations simply do not have sufficient spatial and/or temporal resolution to measure this first peak. The second peak occurs at ~ 60 km and yields 13 MR. This value for the intensity when taken together with the dimen-

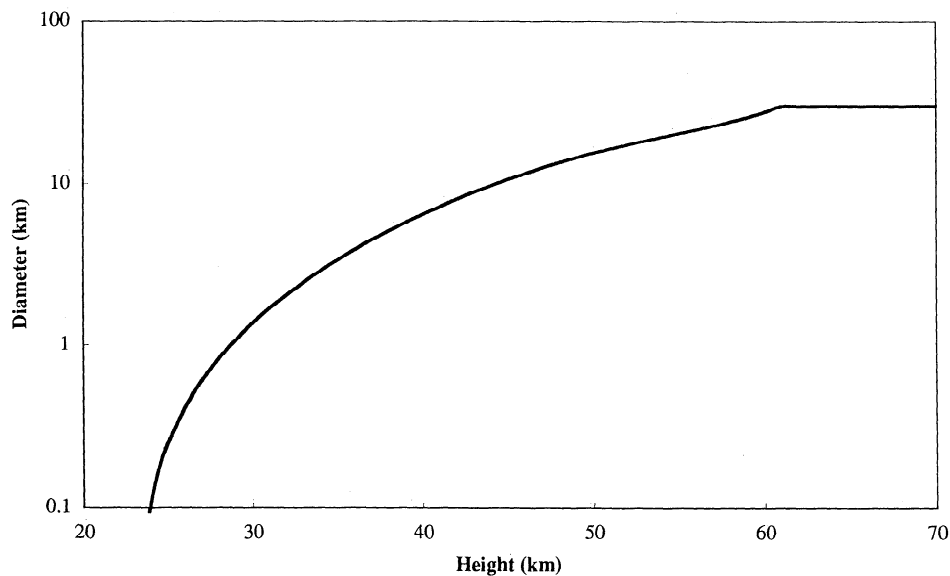


Figure 11. Discharge diameter. The diameter of the discharge region is plotted as a function of height.

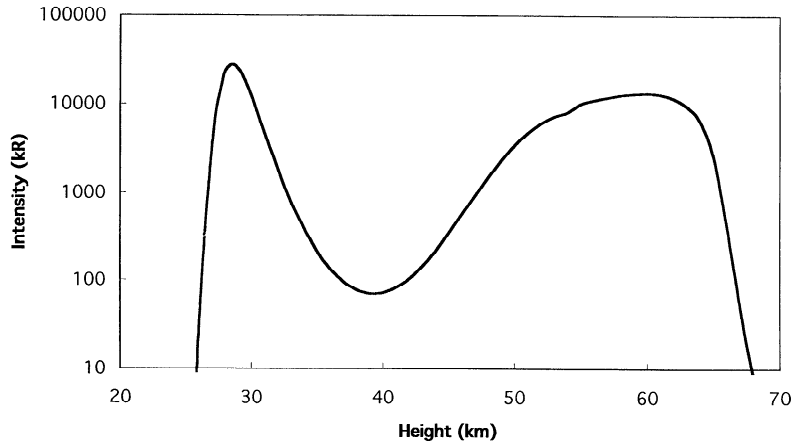


Figure 12. Optical intensity. The computed optical intensity is plotted as a function of height.

sions ($28 \text{ km} \times 10 \text{ km}$) and the emission timescale ($t = 25 \text{ } \mu\text{s}$) yields a total energy of 450 J in basic agreement with the imposed value of 500 J. The early observations of sprites [e.g., *Sentman and Wescott, 1993*] could not resolve the temporal profile of the emissions, while more recent measurements [*Winckler et al., 1994*] still do not have a sufficient combination of spatial and temporal resolution to permit a detailed comparison with the intensities computed here. However, the photometric data taken with $10\text{-}\mu\text{s}$ resolution have shown fine structure down to $100 \text{ } \mu\text{s}$, as would be expected based on our model, and durations of 1–10 ms (see also *Sentman et al. [1995]*), which is longer than those computed here. In addition, the total optical energy has recently been measured to be closer to several kilojoules [*Sentman et al., 1995*]. The additional energy and extended emission time relative to our calculations are most probably associated with the continuing current of secondary electrons in the presence of the thunderstorm electric field. The secondary electron temperature can be obtained from swarm data [see *Ali, 1986*]. For the electric field value at 60 km the mean secondary electron energy is $\varepsilon_s = 1.5 \text{ eV}$. The secondary electron density n_s , as noted in section 2 is equal to $\varepsilon_p/\varepsilon_i$ times the density of primaries. Thus $n_s = (\varepsilon_p/\varepsilon_i)N/V$, where V is the volume of the discharge and N is the total number of primary electrons. At 60-km altitude we obtain an electron density of $n_s = 10^3 \text{ cm}^{-3}$. At these energies and densities there can be substantial optical radiation [e.g., *Taranenko et al., 1993b*]. The fastest timescale for decay of emissions associated with the secondary electrons (including the effects of attachment and recombination) is defined by the conductivity resulting from the secondary electrons themselves. For a collision-dominated plasma the conductivity is simply $\sigma = n_s e^2 / m_e v_{en}$, where v_{en} is the electron-neutral collision frequency. With $v_{en} \text{ (Hz)} = 5.3 \times 10^9 p$ (p is atmospheric pressure in torr) we obtain a relaxation timescale of 1 ms in excellent agreement with recent observations. A quantitative assessment of the additional energy associated with the continuing current of secondary electrons is beyond the scope of this paper. The remaining discrepancy between the several-kilojoule measured optical energy and the model could be resolved by increasing the number of avalanche lengths (lowering the start altitude). Thus, depending on the magnitude of additional optical emissions produced by the secondary current, renormalization of the model could lead to better agreement with the measurements.

The γ ray flux is obtained directly from Figure 5b. Note that the spectrum peaks at approximately 70 keV and subsequently falls off with gamma energy as $\varepsilon^{-1.75}$ to approximately 2 MeV. The emission also falls off sharply with increasing angle from the vertical, primarily because of increased absorption. Integrating the spectrum over energy and multiplying by the BATSE detector area of 2000 cm^2 , we calculate that a total of between 1400 and 40,000 photons would reach the detector in 0.1 ms, depending on the angle of the observer. This result would more than account for the measurements. We also calculate a total duration of approximately 0.17 ms for the discharge, in good agreement with the BATSE measurement of approximately 0.1 ms for the risetime of their events. The longer duration of the BATSE pulses (1–3 ms) is most probably a result of photon scattering by the atmosphere, an effect not included in our calculations.

The results for the radio frequency emissions are shown in Figure 13, in which we plot the total radial Poynting flux (equation (5)) observed by a satellite receiver at a distance of 800 km and positioned at an angle $\theta = 45^\circ$ from vertical as a function of time. Note that η in equation (5) can be written $\eta = vt$ and that the time t in turn is given by $t = (H - H_s) / (1 - \beta_p \cos \theta) / v_p$, where H is the altitude of the discharge (electron beam) and H_s is the start altitude of the discharge. One salient feature of these calculations is the obvious presence of two pulses, as would be seen by a receiver whose noise environment yields a signal-to-noise ratio (or whose dynamic range is) less than 40 dB. The first pulse is produced by the onset of the discharge at low altitudes where the avalanche lengths are small and the corresponding avalanche rates are high. The second pulse is produced by the rapid increase in δ_0 , which leads to large increases in the avalanche rate in spite of the declining atmospheric pressure. The duration of the signal depends on the SNR but would typically not exceed several microseconds for the first pulse. The duration of the second pulse is longer, but this result depends strongly on the conductivity profile, which is not well known, particularly in the transition region around 50 to 70-km altitude, above which the formation of the ionospheric D region begins. The separation of the pulses in time is seen in this case to be approximately 34 μs . Recall that all of these times depend on the angle of the receiver relative to vertical. The peak fluence F_{VHF} in the VHF band above $f = 25 \text{ MHz}$ was calculated for the first pulse by taking a Fourier transform of the radiated electric field

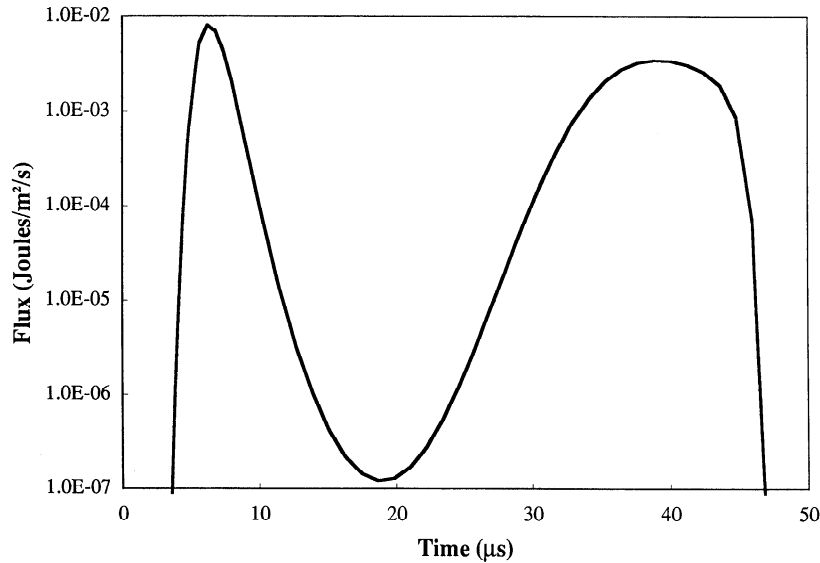


Figure 13. Sprite radio emissions. The total Poynting flux for the electromagnetic radiation produced by a runaway upward discharge is plotted as a function of time in the frame of reference of an observer located at 800 km from the source and at an angle of 45° relative to the vertical.

profile corresponding to the flux shown in Figure 13, multiplying by the complex conjugate, and integrating above 25 MHz. Because the temporal shape of the radiated field is not simply exponentiating in time, the spectrum falls off as $1/f^2$ instead of $1/f$ as discussed in the previous section. The peak fluence was found to be $F_{\text{VHF}} = 1.1 \times 10^{-14} \text{ J/m}^2$. This result is directly proportional to the optical energy used to normalize the model and depends strongly on the angle of the receiver relative to vertical (see equation (5)). The second pulse has an amplitude a factor of 60 less than the first; however, this result is strongly dependent on the conductivity of the atmosphere. To illustrate this fact, we decreased the conductivity by a factor of 2 in the region 40–70 km and recomputed the radio frequency emissions. The results are shown in Figure 14b with the corresponding electric field profile shown in Figure 14a. The peak flux in the second pulse now exceeds the first by a factor of 15, and the maximum is shifted to a later time (or higher altitude). In addition, we obtain a sharply decreasing amplitude for times greater than $50 \mu\text{s}$. This component enhances significantly the high-frequency emissions. Thus the conductivity plays a significant role in defining the electric field profile, which in turn determines the associated optical, γ ray, and RF emissions. We note that the strong forward directed nature of the radio emissions would explain why these pulses are not as easily identified from the ground. Finally, the reflection of a lightning spheric by the ground has been advanced as a potential explanation for the second pulse observed by Blackbeard. However, as pointed out by *Massey and Holden* [1995], at VHF frequencies the ground becomes a poor reflector with irregularity scale lengths of the same order as the wavelength. Thus it would be difficult with a reflection hypothesis to explain the fact that the second pulse is observed to be brighter than the first in 30% of the measurements. The basic qualitative and quantitative results of our model are in excellent agreement with the observations of TIPP events obtained by the Blackbeard experiment [*Holden et al.*, 1995; *Massey and Holden*, 1996]. More detailed calculations to examine the precise effects of the atmospheric conductivity are left for future more comprehensive studies.

The results obtained in our rough model are strongly dependent on the magnitude and configuration of the electric field, and a number of different scenarios are possible. However, the basic shape of the normalized field, namely, a dip at intermediate altitudes (30–40 km) followed by a rise to higher altitudes and a subsequent decline above 65–70 km (due to the rapid rise in air conductivity), will remain the same and in the context of runaway breakdown is the primary ingredient for the development of a double pulse in the VHF with the measured temporal characteristics of several microseconds in width and tens of microseconds in pulse separation. In addition, for weaker charge neutralization the field can dip below the threshold for runaway breakdown, and therefore the region between 30 and 40 km marks a natural separation point for the development of blue jets versus sprites, as observed in the optical, in agreement with the observations [*Wescott et al.*, 1995].

As noted previously, the geomagnetic field becomes important at low geomagnetic latitude and high altitudes. While the bulk of the optical measurements were taken at midlatitudes where the effect of the magnetic field is minimal, it is nevertheless worthwhile to comment on potential effects at other locations. We have omitted the field in our model only because of the lack of available kinetic computations for the parameter space of interest. However, we do not believe that the magnetic field will alter the basic characteristics of the model. First, the runaway beam develops primarily at altitudes below 40 km, where collisions dominate. It is from this altitude range that the bulk of the optical intensity and γ ray emissions as well as the first radio pulse originate. At higher altitudes we see that the normalized electric field (δ_0) increases rapidly, causing the critical altitude at which magnetic field effects become important to increase to 50–60 km. In the intermediate regime, between the collision-dominated and magnetic field dominated regimes, the avalanche rate will be enhanced over that used in our model, and this effect will help to carry the beam to higher altitudes, where the larger normalized fields exist. The enhanced ionization rate will also contribute to an increase in the

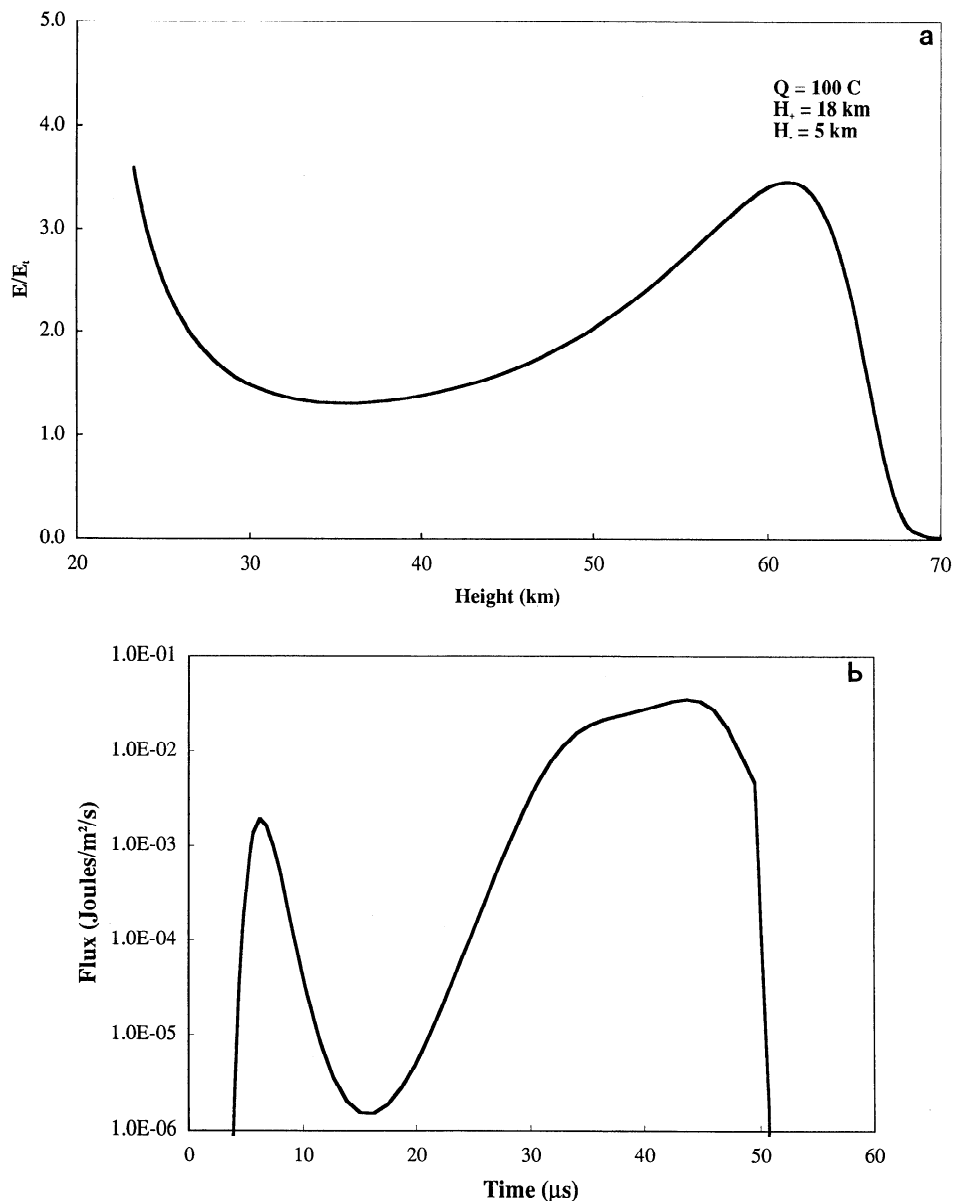


Figure 14. Sprite radio emissions with reduced atmospheric conductivity. (a) The normalized electric field under the same conditions described in Figure 9 but with the nighttime atmospheric conductivity (shown in Figure 8) enhanced by a factor of 2 between 40 km and 70 km plotted as a function of height. (b) The corresponding total Poynting flux for the electromagnetic radiation produced by a runaway upward discharge plotted as a function of time.

amplitude of the second radio pulse at lower altitudes. The precise magnitude of these effects will have to be determined in future more comprehensive models.

Recent attempts to account for the optical flashes termed sprites have been based primarily on conventional breakdown of the air, either as a result of large-amplitude (greater than hundreds of volts per meter at 70-km altitude or greater than tens of volts per meter at 100 km) electromagnetic pulses launched by strong (producing currents in excess of tens of kiloamperes) horizontal lightning strikes [Taranenko *et al.*, 1993a, b; Milikh *et al.*, 1995; Rowland *et al.*, 1995] or as a result of quasi-static electric field changes caused by strong lightning strikes [Pasko *et al.*, 1995]. The advantages of the runaway model are numerous. The threshold electric field needed to initiate runaway air breakdown is a factor of 10 less than that

required for conventional breakdown. As a result the runaway mechanism will proceed first under any electric field configuration that has sufficient scale lengths (tens to hundreds of meters). The magnitude and morphology of the optical emissions computed with our model are more in line with the observations. None of the models based on conventional breakdown shows emissions below about 65-km altitude, in direct contradiction with the observations. In the case of runaway breakdown, most of the avalanching takes place below 30 km (see Figure 10), so that the beam is well developed by this point, and as a result, substantial optical emissions exist starting at 25–30 km. A recent one-dimensional model based on runaway breakdown was developed by Bell *et al.* [1995]. Their results indicate that in order to reproduce the observed intensity of red sprites, a minimum of 250 C would have to be

Table 2. Comparison of Model With Observations

	Model	Observations
Total optical energy	fixed to measurements (500 J)	~100 J to several kJ
Optical intensities	13 MR at 60 km	10–600 kR (insufficient temporal and spatial resolution)
Optical spectrum	blue dominates at low altitude red dominates at high altitude	blue dominates at low altitude red dominates at high altitude
Maximum diameter	28 km	10–50 km
Altitude of source region	>25 km	25–90 km
Peak gamma flux	7×10^3 – 2×10^5 photons/cm ² /s	100 counts/cm ² /s
Energy of peak gamma flux	70 keV	...
Risetime of gamma pulse	0.17 ms	0.1 ms
Duration of gamma pulse	0.3 ms (enhanced by scattering)	2–5 ms
Tipp duration	several μ s	mean of 5 μ s
Pulse separation	tens of μ s depending on viewing angle	mean of 51 μ s
Radio flux above 25 MHz	1.1×10^{-14} J/m ² at 800 km from source and a 45° angle	median of 1×10^{-14} J/m ²

neutralized in the quasi-electrostatic field model. Our model only requires 100 C with the primary difference between the two being the assumed charge configuration. The runaway model presented here is the first to associate both the BATSE γ ray observations and the Blackbeard radio flashes with the same mechanism that is potentially responsible for sprites. Conventional breakdown cannot account for the γ ray observations, and there is no existing theory (ground reflections aside) for the TIPP events.

4. Summary

The excellent agreement between the observations and our model predictions summarized in Table 2 suggests that runaway breakdown is the driving mechanism for upward discharges and that these discharges are the source of the mysterious radio and γ flashes. Confirmation could be attained by simultaneously measuring the optical, γ , and radio frequency emissions. These measurements, when interpreted with models of the discharge, would provide a wealth of information on thunderstorm electricity and its role in coupling to the upper atmosphere and the overall global circuit.

If our analysis is correct, then upward discharges represent the first known manifestation of a fundamental, new process in plasma physics. Observations of these spectacular natural phenomena offer us an excellent opportunity to verify the theoretical predictions of runaway air breakdown.

Acknowledgments. The authors would like to thank Tom Tunnell (EG&G Energy Measurements, Los Alamos, New Mexico) for helpful discussions regarding the estimates obtained for radio frequency emissions from the runaway mechanism. We gratefully acknowledge numerous interesting and important conversations with William Feldman (Los Alamos National Laboratory) regarding runaway breakdown and the corresponding γ ray emissions. Similar useful discussions on radio and γ ray emissions were also held with William Armstrong, David Susczynsky, and Robert Massey (Los Alamos National Laboratory). We are also thankful to Dave Sentman for constructive and detailed criticism of this paper. This work was performed under the auspices of the U.S. Department of Energy and funded in part by the Laboratoire de Détection et de Géophysique, Commissariat à l'Énergie Atomique, France.

The Editor thanks three referees for their assistance in evaluating this paper.

References

- Ali, A. W., Intense and short electric field (dc and microwave) air-breakdown parameters, *Memo. Rep.* 5015, Natl. Res. Lab., Washington, D. C., 1986.
- Bell, T. F., V. P. Pasko, and U. S. Inan, Runaway electrons as a source of red sprites in the mesosphere, *Geophys. Res. Lett.*, **22**, 2127, 1995.
- Bethe, H. A., Theory of passage of swift corpuscular rays through matter, *Ann. Phys.*, **5**, 325, 1930.
- Bethe, H. A., and J. Ashkin, Penetration of beta-rays through matter, in *Experimental Nuclear Physics*, vol. 1, edited by E. Segre, p. 277, John Wiley, New York, 1953.
- Blakeslee, R. J., H. J. Christian, and B. Vonnegut, Electrical measurements over thunderstorms, *J. Geophys. Res.*, **94**(D11), 13,135, 1989.
- Boccippio, D. J., E. R. Williams, S. J. Heckman, W. A. Lyons, I. T. Baker, and R. Boldi, Sprites, ELF transients, and positive ground strokes, *Science*, **269**, 1088, 1995.
- Boeck, W. L., O. H. Vaughan Jr., and R. J. Blakeslee, Low light level television images of terrestrial lightning as viewed from space (abstract), *Eos Trans. AGU*, **72**, 171, 1990.
- Boeck, W. L., O. H. Vaughan Jr., R. J. Blakeslee, B. Vonnegut, M. Brook, and J. McKune, Observations of lightning in the stratosphere, *J. Geophys. Res.*, **100**(D1), 1465, 1995.
- Boys, C. V., Progressive lightning, *Nature*, **118**, 749–750, 1926.
- Davidson, G., and R. O'Neil, Optical radiation from nitrogen and air at high pressure excited by energetic electrons, *J. Chem. Phys.*, **41**(12), 3946, 1964.
- Everett, J. D., and W. H. Everett, Rocket lightning, *Nature*, **68**, 599, 1903.
- Fisher, J. R., Upward discharges above thunderstorms, *Weather*, **45**, 451, 1990.
- Fishman, G. J., et al., Discovery of intense gamma-ray flashes of atmospheric origin, *Science*, **264**, 1313, 1994.
- Franz, R. C., R. J. Nemzek, and J. R. Winckler, Television image of a large upward electrical discharge above a thunderstorm system, *Science*, **249**, 48, 1990.
- Gales, D. M., Lightning to the ionosphere: Another account, *Weatherwise*, **35**, 72, 1982.
- Gurevich, A. V., G. M. Milikh, and R. A. Roussel-Dupré, Runaway electron mechanism of air breakdown and preconditioning during a thunderstorm, *Phys. Lett. A*, **165**, 463, 1992.
- Gurevich, A. V., G. M. Milikh, and R. A. Roussel-Dupré, Nonuniform runaway air-breakdown, *Phys. Lett. A*, **187**, 197, 1994.
- Hartman, K. B., New measurement of the fluorescence efficiency of air under electron bombardment, *Planet. Space Sci.*, **16**, 1315, 1968.
- Holden, D. N., C. P. Munson, and J. C. Devenport, Satellite observations of transitionospheric pulse pairs, *Geophys. Res. Lett.*, **22**, 889, 1995.
- Krchbiel, P. R., The electrical structure of thunderstorms, in *The Earth's Electrical Environment*, p. 206, Natl. Acad. Press, Washington, D. C., 1986.

- Lyons, W. A., Characteristics of luminous structures in the stratosphere above thunderstorms as imaged by low-light video, *Geophys. Res. Lett.*, 21(10), 875, 1994.
- Lyons, W. A., and E. R. Williams, Preliminary investigations of the phenomenology of cloud-to-stratospheric lightning discharges, paper presented at 17th Conference on Severe Local Storms/Conference on Atmospheric Electricity, Am. Meteorol. Soc., St. Louis Mo., Oct. 4–8, 1993.
- Lyons, W. A., J. R. Winckler, R. J. Nemzek, P. R. Malcolm, E. R. Williams, and D. Boccippio, The 1994 Colorado SPRITE campaign: Initial results, (abstract) *Eos Trans. AGU*, 75(44), Fall Meet. Suppl., 108, 1994.
- Malan, D., Sur les décharges orageuses dans la haute atmosphère, *C. R. Acad. Sci. Paris*, 205, 812, 1937.
- Marshall, T. C., and W. D. Rust, Electric field soundings through thunderstorms, *J. Geophys. Res.*, 96(D12), 22,297, 1991.
- Massey, R. S., and D. N. Holden, Phenomenology of transionospheric pulse pairs, *Radio Sci.*, 30(5), 1645, 1995.
- McCarthy, M. P., and G. K. Parks, On the modulation of X ray fluxes in thunderstorms, *J. Geophys. Res.*, 97(D5), 5857, 1992.
- Milikh, G. M., K. Papadopoulos, and C. L. Chang, On the physics of high-altitude lightning, *Geophys. Res. Lett.*, 22, 85, 1995.
- Mitchell, K. B., Fluorescence efficiencies and collisional deactivation rates for N_2 and N_2^+ bands excited by soft X rays, *J. Chem. Phys.*, 53(5), 1795, 1970.
- Pasko, V. P., U. S. Inan, Y. N. Taranenko, and T. F. Bell, Heating, ionization, and upward discharges in the mesosphere due to intense quasi-electrostatic thundercloud fields, *Geophys. Res. Lett.*, 22(16), 2127, 1995.
- Roussel-Dupré, R. A., and R. H. Miller, Kinetic theory of runaway air breakdown with a magnetic field (abstract), *Eos Trans. AGU*, 75(44), Fall Meet. Suppl., 148, 1994.
- Roussel-Dupré, R. A., A. V. Gurevich, T. Tunnell, and G. M. Milikh, Kinetic theory of runaway air breakdown and the implications for lightning initiation Rep. LA-12601-MS, Los Alamos Natl. Lab., Los Alamos, N. M., 1993.
- Roussel-Dupré, R. A., A. V. Gurevich, T. Tunnell, and G. M. Milikh, Kinetic theory of runaway air breakdown, *Phys. Rev. E*, 49(3), 2257, 1994.
- Rowland, H. L., R. F. Fernsler, J. D. Huba, and P. A. Bernhardt, Lightning-driven EMP in the upper atmosphere, *Geophys. Res. Lett.*, 22(4), 361, 1995.
- Sentman, D. D., and E. M. Wescott, Observations of upper atmospheric optical flashes recorded from an aircraft, *Geophys. Res. Lett.*, 20, 2857, 1993.
- Sentman, D. D., E. M. Wescott, D. L. Osborne, D. L. Hampton, and M. J. Heavner, Preliminary results from the Sprites94 aircraft campaign, 1, Red sprites, *Geophys. Res. Lett.*, 22, 1205, 1995.
- Taranenko, Y. N., and R. Roussel-Dupré, High altitude discharges and gamma-ray flashes: A manifestation of runaway air breakdown, *Geophys. Res. Lett.*, in press, 1996.
- Taranenko, Y. N., U. S. Inan, and T. F. Bell, Interaction with the lower ionosphere of electromagnetic pulses from lightning: Heating, attachment, and ionization, *Geophys. Res. Lett.*, 20(15), 1539, 1993a.
- Taranenko, Y. N., U. S. Inan, and T. F. Bell, Interaction with the lower ionosphere of electromagnetic pulses from lightning: Excitation of optical emissions, *Geophys. Res. Lett.*, 20(23), 2675, 1993b.
- Uman, M. A., *Lightning*, Dover, Mineola, N. Y., 1984.
- Vaughan, O. H., Jr., and B. Vonnegut, Recent observations of lightning discharges from the top of a thundercloud into the clear air above, *J. Geophys. Res.*, 94(D11), 13179, 1989.
- Vaughan, O. H., Jr., Observations of nocturnal thunderstorms and lightning displays as seen during recent space shuttle missions, paper presented at 17th Conference on Severe Local Storms/Conference on Atmospheric Electricity, Am. Meteorol. Soc., St. Louis Mo., Oct. 4–8, 1993.
- Vaughan, O. H., Jr., R. J. Blakeslee, W. L. Boeck, B. Vonnegut, M. Brook, and J. McKune Jr., A cloud-to-space lightning as recorded by the space shuttle payload-bay TV cameras, *Mon. Weather Rev.*, 120(7), 1459, 1992.
- Wescott, E. M., D. D. Sentman, D. L. Osborne, D. L. Hampton, and M. J. Heavner, Preliminary results from the Sprites94 aircraft campaign, 2, Blue jets, *Geophys. Res. Lett.*, 22, 1209, 1995.
- Wilson, C. T. R., The electric field of a thundercloud and some of its effects, *Proc. R. Soc. London*, 37, 32D, 1925.
- Wilson, C. T. R., A theory of thundercloud electricity, *Proc. R. Soc. London*, 236, 297, 1956.
- Winckler, J. R., R. C. Franz, and R. J. Nemzek, Fast low-level light pulses from the night sky observed with the SKYFLASH program, *J. Geophys. Res.*, 98(D5), 8775, 1993.
- Winckler, J. R., W. A. Lyons, and R. J. Nemzek, New high-resolution ground-based studies of cloud-ionosphere discharges (CIs) (abstract), *Eos Trans. AGU*, 75(44), Fall Meet. Suppl., 107, 1994.
- Winn, W. P., G. W. Schwede, and C. B. Moore, Measurements of electric fields in thunderclouds, *J. Geophys. Res.*, 79(12), 1761, 1974.
- Winn, W. P., C. B. Moore, and C. R. Holmes, Electric field structure in an active part of a small, isolated thunderstorm, *J. Geophys. Res.*, 86(C2), 1187, 1981.

A. V. Gurevich, P. N. Lebedev Institute of Physics, Moscow 117924, Russia. (e-mail: gurevich@linaxl.dnet.gwdg.de)

R. Roussel-Dupré, Space and Atmospheric Sciences Group, Los Alamos National Laboratory, NIS-1, M. S. d-466, Los Alamos, NM 87545. (e-mail: rroussel-dupre@lanl.gov)

(Received March 20, 1995; revised October 19, 1995; accepted October 24, 1995.)